

Communication

Digital Non-Linear Transmitter Equalization for PAM-N-Based VCSEL Links Enabling Robust Data Transmission of 100 Gbit/s and Beyond

Urs Hecht ^{1,*} , Nikolay Ledentsov, Jr. ² , Helia Ordouei ¹ , Patrick Kurth ¹ , Philipp Scholz ¹ ,
Nikolay Ledentsov ²  and Friedel Gerfers ¹ ¹ Chair of Mixed Signal Circuit Design, Technische Universität Berlin, Einsteinufer 17, 10587 Berlin, Germany² Vertically Integrated Systems GmbH (VIS), Hardenbergstraße 7, 10623 Berlin, Germany

* Correspondence: hecht@tu-berlin.de; Tel.: +49-30-314-25882

Abstract: This paper demonstrates why VCSEL-based transmitter systems are not able to capitalize on higher-order PAM modulation formats (such as PAM-4) to push the link data rate towards 100 Gbit/s with BER of better than 10^{-5} . First, the non-linear and biasing-dependent VCSEL behavior is analyzed in great detail to prove why state-of-the-art VCSELs with linear equalization are not able to reach these bandwidth targets. Consequently, based on an enhanced VCSEL model, a digital non-linear transmit equalizer is proposed to overcome voltage-dependent relaxation frequency shifts as well as data-dependent VCSEL bandwidth variations. The proposed digital non-linear equalizer is compared with a standard linear FFE structure using PAM-4 transmission experiments of 100 Gbit/s and beyond. This way, the proposed non-linear equalizer reveals a BER improvement of more than 30-fold compared to a linear FFE at a data rate of 80 Gbit/s. Finally, at 112 Gbit/s PAM-4 the non-linear equalizer was successfully demonstrated at a BER of $1.5 \cdot 10^{-7}$.

Keywords: optical fiber transmission; VCSEL; voltage-dependent relaxation frequency shifts; biasing-dependent VCSEL bandwidth variations; linear FFE; digital non-linear transmit equalization



Citation: Hecht, U.; Ledentsov, N., Jr.; Ordouei, H.; Kurth, P.; Scholz, P.; Ledentsov, N.; Gerfers, F. Digital Non-Linear Transmitter Equalization for PAM-N-Based VCSEL Links Enabling Robust Data Transmission of 100 Gbit/s and Beyond. *Photonics* **2023**, *10*, 280. <https://doi.org/10.3390/photonics10030280>

Received: 31 January 2023

Revised: 25 February 2023

Accepted: 2 March 2023

Published: 7 March 2023



Copyright: © 2023 by the authors. Licensee MDPI, Basel, Switzerland. This article is an open access article distributed under the terms and conditions of the Creative Commons Attribution (CC BY) license (<https://creativecommons.org/licenses/by/4.0/>).

1. Introduction

Since the rise of modern short- to mid-range communication systems, innovation and advancements in this field (mobile services, radar, Internet-of-Things (IoT) and optical communication systems) heavily rely on the availability of high-speed transceivers. The total amount of data transferred increased exponentially to 122 exabyte per month by 2017, while it was expected to reach over 396 exabyte per month by 2022 [1]. Although this development calls for even faster networking equipment, the energy and cost efficiency of the devices also starts to be equally important. Low energy efficiency leads to several problems on all architectural levels, from thermal management (when dealing with high integration), to higher operating costs, to the toll on the environment. Vertical-Cavity Surface-Emitting Laser (VCSEL) diodes [2–5] are known to be much more cost and energy-efficient at converting electrical signals into optical signals than alternative optical sources or modulators, such as Mach-Zehnder-Modulators (MZMs) or Electro-Absorption Modulated Lasers (EMLs). However, the gain in power efficiency for VCSEL-based transmitter systems is much smaller than expected as the VCSEL-driver dominates the overall power budget.

The obtained data rates of recently published VCSEL transmit systems are plotted in Figure 1a. Although the average data rate has increased over the years, both for Non-Return to Zero (NRZ) and Pulse Amplitude Modulation (PAM)-modulated systems, no significant improvement of the State-of-the-Art (SOTA) data rate has been achieved since the publishing of [6] at 71 Gbit/s in 2014. It should be noted that the link with the highest published data rate [7] still uses NRZ modulation even though the PAM-4 modulation scheme should ideally increase the data rate by 2x when considering the same system

bandwidth. Although 100 Gbit/s optical Multi-Mode Fiber (MMF) transmission standardization is finalized [8] with companies claiming products capable of this performance [9], published VCSEL transmitter systems using PAM-4 signaling only reached data rates of 60 Gbit/s such as [10–12]. As can be seen in Figure 1b, the most efficient VCSEL transmitters are also still using NRZ modulation. Although VCSELs are very energy-efficient, they suffer from limited bandwidth, a frequency response with current-dependent resonant behavior leading to overshoots as well as non-linear rise-and-fall times, which significantly impairs the Bit-Error Rate (BER) using PAM-4 modulation schemes. This paper aims to demonstrate PAM-4-based equalization techniques that can easily be implemented into Digital-to-Analog Converter (DAC)-based transmitters, enabling transmission at over 100 Gbit/s reaching efficiencies common for copper-based transmitter systems. This scheme could also easily be extended to be used with PAM-6 or even PAM-8 modulation.

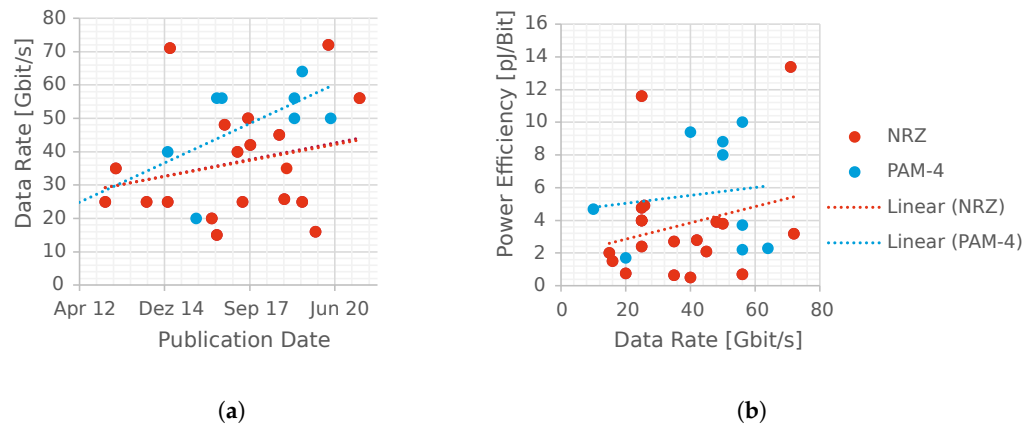


Figure 1. VCSEL Transmitter System (a) data rates over publication dates (b) power efficiency.

2. Non-Linear VCSEL Behavior

All directly modulated LASERS (and therefore also VCSELs) exhibit non-linear behavior in their frequency response when varying the operation current, which happens with every change of the data symbol i.e., changing the optical power level. Figure 2 shows the measured frequency response of a VCSEL [2] for different bias currents. It is evident that the VCSEL exhibits biasing-dependent resonance frequency shifts and non-linear bandwidth reduction that influences its frequency response and data transmission.

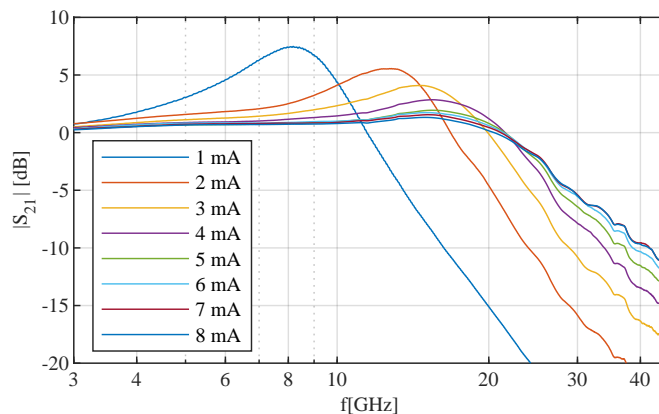


Figure 2. Frequency response of VCSEL for different bias currents.

At low currents, the resonance is very distinct, causing strong Inter Symbol Interference (ISI). To obtain a flatter frequency response and avoid strong resonances, VCSELs are usually biased above 3 mA. For higher currents, the resonances become increasingly less pronounced. However, larger VCSEL bias currents inherently cause self-heating effects

in turn limiting the VCSEL's bandwidth [3] or (when surpassing operating thresholds) damaging the device. It is important to note that the measurements performed for Figure 2 were executed at a constant bias current (so in a high self-heating state). In reality the VCSEL might exhibit such high currents only for very short duration, meaning that the VCSEL does not experience self-heating effects as severely due to its dynamic signaling. Because of this, the VCSEL can reach higher bandwidths than the Alternating Current (AC) measurements reveal.

Because the AC-response measurement is somewhat limited for explaining VCSEL behavior, the so-called pulse response of a VCSEL is shown in Figure 3. The pulse response is very similar to an impulse response, the only difference is that 1 Unit Interval (UI) wide pulses are used. A PAM-4 modulated signal has 16 different possible data transition combinations for two consecutive data sets, of which four do not cause a modulation level change. Thus, these four Direct Current (DC) cases are omitted leaving 12 different data transitions. Please note that a different VCSEL was used for AC and pulse response measurement due to test setup and assembly. It becomes evident from Figure 3 that the VCSEL does not have sufficient bandwidth to transmit 56 Gbaud as the pulses are not reaching the DC values during the transition. Moreover, the data-dependent relaxation oscillations (different per output level) are clearly visible, contributing to the ISI and BER problem. The oscillations vary both in frequency and amplitude. This means that commonly used Finite Impulse Response (FIR)/Feed-Forward Equalizer (FFE) filtering is not effective for VCSEL equalization, since the filter operates in a linear fashion such that the coefficients can only be optimized for one of the responses, not all of them.

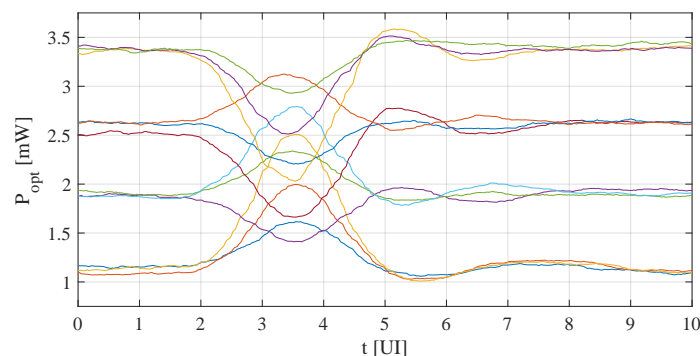


Figure 3. All 12 possible PAM-4 pulse responses at a symbol rate of 56 Gbaud.

Figure 3 also shows that the top eye will be more shifted to the left (so earlier in time) and the bottom eye more shifted to the right (so later in time) than the middle eye. This effect, called skewing, is due to the asymmetric rise-and-fall times of the VCSEL (originating from current-dependent bandwidth) and severely increases the BER of a transceiver system. It can only be prevented by non-linear filtering (like Volterra or the one proposed in this paper) or by having a specialized receiver with independent slicing times for all three PAM-4 eyes.

To acquire a deeper understanding of VCSEL behavior, we introduce an accurate electro-optical VCSEL model [13]. The model used is shown in Figure 4, where the discrete components of the electronic interface are summarized in Table 1.

The electronic interface consists of linear, passive components, mainly modelling parasitic (pad) capacitances, inductances, non-linear diode behavior as well as the non-linear active area impedance of the LASER. The equivalent current through the active area $I(t)$ serves as an input for the rate equations. The rate equations can be used to describe the behavior of the LASER (edge emitting and VCSEL). As it is a set of differential equations, they describe the derivation of the carrier density $n(t)$ and the photon density $N(t)$. Solving the rate equations enables the estimation of the photon density, which is proportional to the optical output power. Since the current through the active area is a

coefficient of the differential equation, the VCSEL exhibits non-linear behavior when the current is modulated.

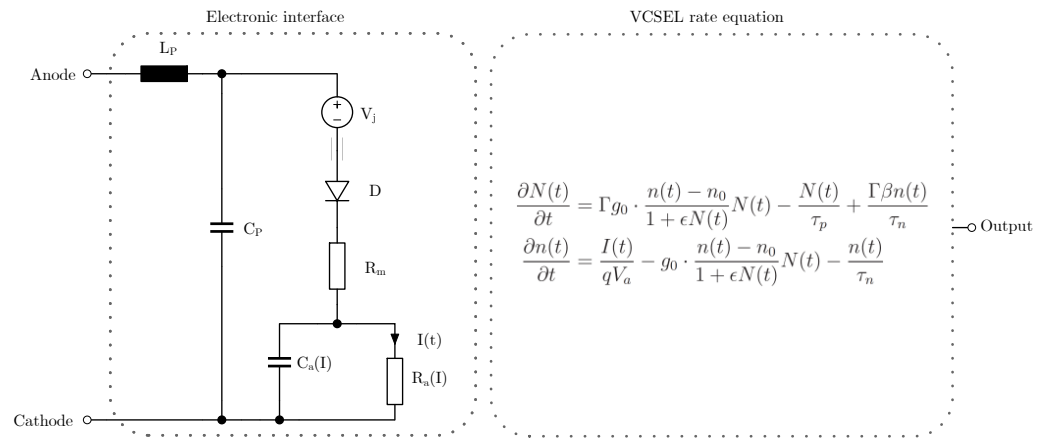


Figure 4. VCSEL equivalent circuit [13].

Table 1. Components of electronic interface.

Component	Unit	Description
L_p	H	Series inductance of pad connection
C_p	F	Parasitic pad capacitance
R_m	Ω	Mirror resistance
R_a	Ω	Active area resistance
C_a	F	Active area capacitance
V_j	V	Intrinsic diode voltage
I_s	A	Diode reverse saturation current
n	-	Diode ideality factor

The parameters are extracted by fitting model behavior to measurement data. One of the formulas used is given in Equation (1), with f_r being the resonant frequency, I being the VCSEL operating current and I_{th} being the threshold current of the VCSEL.

$$f_r = \frac{\sqrt{B(I - I_{th})}}{2\pi} \tag{1}$$

When trying to increase the data rate of a VCSEL-based transmission system, two approaches are possible: One either increases the baud rate, which is only possible if the bandwidth of the components is also increased. Knowing that the bandwidth of the VCSEL f_{3db} is proportional to the resonance frequency f_r , it is only possible by designing the VCSEL in a way so the rate equation parameter B (with the unit $s^{-2}A^{-1}$ [14]) is increased, which in turn would mean that the difference in resonance frequencies Δf_r also has to increase. The other possibility is to switch from lower order modulation (like NRZ) to higher-order (like PAM-4 or PAM-8), which comes at the drawback of needing larger signal amplitudes for similar error rates. This is only possible by increasing the modulation current amplitude ΔI , which in turn also increases Δf_r . Hence, specialized filtering for non-linear VCSEL behavior becomes increasingly important and is discussed in the following chapter.

3. Equalization Schemes

The most common linear equalization filter structure used in transmitters is the Feed-Forward Equalizer, as shown in Figure 5. It is basically an FIR filter and works by shaping the pulse response in such a way that, in the optimal case, all pre- and post-cursors are reduced to zero, eliminating all ISI.

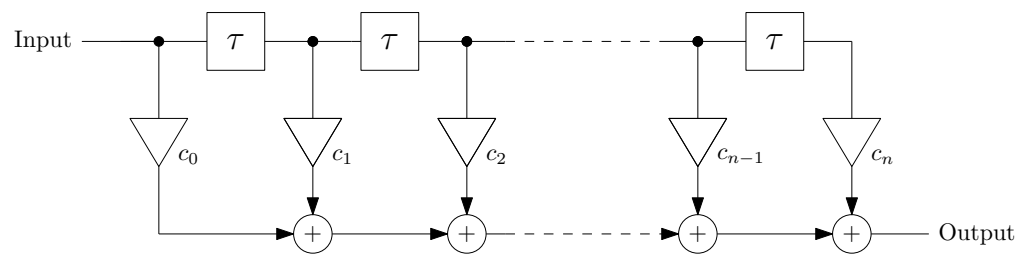


Figure 5. Block diagram of a n tap FFE.

FFEs are very popular because of the simple and wide range of implementation architectures. The delay elements can be implemented either with synchronously clocked flip-flops, transmission lines or by analog delay elements. The summing and scaling of coefficients can be implemented by parallel connection of scaled switched current sources either before or inside the final driver. Alternatively, the filter functions can be realized in the digital domain (as an FIR either through an equivalent circuit or a simple Lookup Table (LUT)) which is then followed by a DAC-driver.

As previously discussed, FFEs are not able to filter the relaxation oscillations for all biasing and input data conditions. It was demonstrated that 112 Gbit/s PAM-4 VCSEL data transmission is possible with the use of a Volterra non-linear equalizer [15,16]. However, the implementation of a Volterra filter requires a power-hungry digital signal processor and cannot easily be implemented in the output driver, as would be the case with an FFE. A much more efficient technique is to dynamically adapt FFE coefficients based on the input data. Adaptive, UI-based FFE pre-emphasis was already implemented for NRZ-modulated signaling [17–19]. These filters are made adaptive by switching the tap coefficients based on current and subsequent NRZ digital values. This is simple as only two code levels have to be considered. It is debatable though if these filter structures are really necessary for NRZ transmission, since an asymmetric data eye is not a problem as long as the BER is sufficiently low. On the contrary, for higher PAM modulation formats, equalization becomes essentially mandatory. The eye amplitude becomes a fraction of the full scale signal, overshoots can decrease the size of adjacent eyes and asymmetric rise-and-fall times have a much more severe effect.

A proposal for an adaptive PAM-4 FFE [20] is shown in Figure 6. It works just like a linear FFE, but the actual coefficients $c_{1,x} \dots c_{4,x}$ are selected depending on the state of the main tap 0, 1, 2 or 3 (00b, ..., 11b).

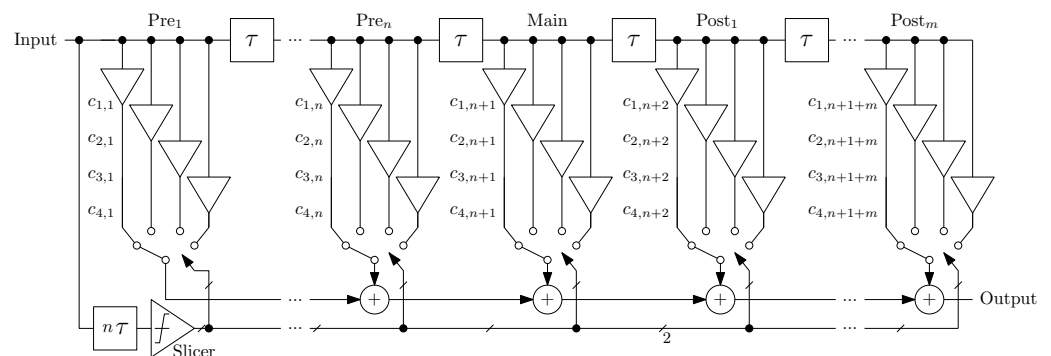


Figure 6. Block diagram of adaptive FFE, n pre and m post-taps, four sets of coefficients for PAM-4 signaling.

As can be seen in Figure 3, the resulting relaxation oscillation amplitude and frequency differs for the four PAM levels. The oscillation frequency ranges from 11 GHz for level 0 to 20 GHz for level 3 (as a result of the bias dependent transfer function shown in Figure 2). The main tap is used to decide on one set of coefficients, as it directly correlates with the operating current, therefore defining the oscillation behavior of the VCSEL. This equalizer design could be incorporated into standard Current-Mode Logic (CML) FFE

implementations as in [11], or as a digital adaptive FIR filter followed by a baud rate current-steering DAC with an extra VCSEL bias current source.

As explained in Section 2, the VCSEL shows different relaxation oscillation frequencies for all 12 possible pulse responses, so linear scaling of the coefficients is expected to improve the BER but leave significant performance boost unused. The digital sample-based topology [20] shown in Figure 7 uses its own set of coefficients for every possible set of pulse responses.

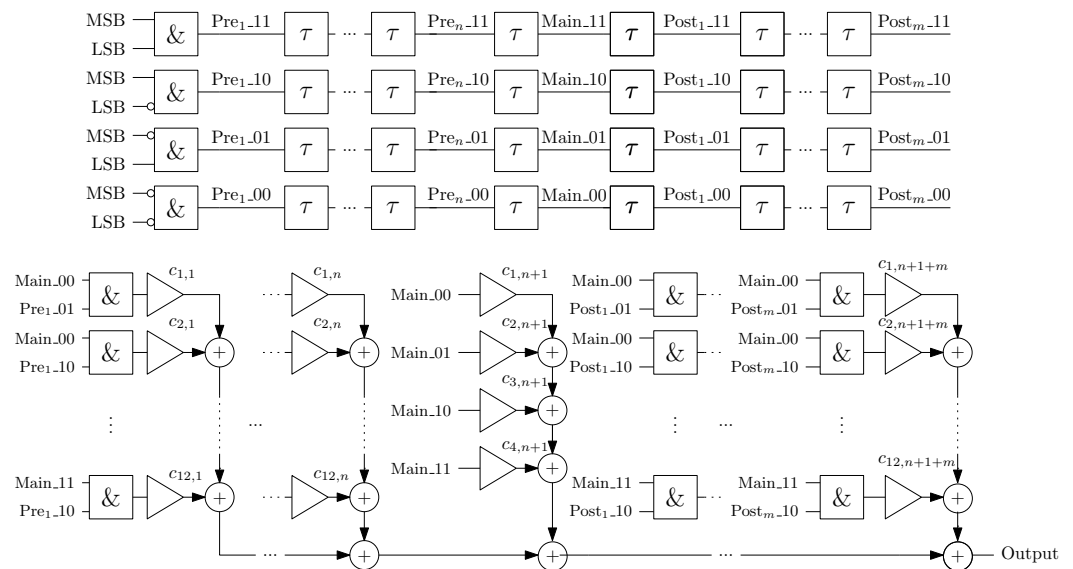


Figure 7. Block diagram of adaptive FFE, n pre and m post-taps, 12 sets of coefficients for PAM-4 signaling.

Each of the four possible combinations of MSB and LSB are split into four lanes of UI-based delay chains. For every tap, only one state within the chains (i.e., $Pre_{1_11}, \dots, Pre_{1_00}$) is logically true. When the state of the main tap is different from one of the other taps, an edge is detected and the corresponding FFE coefficient is added. This topology offers several advantages. First, each of the 12 pulse response combinations can be optimized (almost) independently. They are not totally independent because the height of the peak is dependent on the Pre_1 and $Post_1$ tap coefficients of the level of the peak. Second, the proposed architecture avoids multipliers which are expensive in terms of hardware and delay. Since only one of the tap states is valid, all additions of one tap can be replaced by 16 entries of a LUT. Alternatively, the proposed filter is fully realized by a LUT using 24 inputs (4 states times 6 taps) resulting in 4^6 (i.e., 4096) LUT entries. Because of the complexity of the filter, a digital implementation is more energy-efficient than the analog counterpart. Using a CML approach, the adders would yield a large number of differential pairs in parallel creating an unrealistically high load. Finally, due to the digital nature of the proposed filter, this topology can also easily be extended to a larger amount of taps (at the added cost of complexity in the digital domain and hence larger power draw) as well as to handling PAM-6, PAM-8 or higher modulation formats.

4. Training Sequence

To determine linear FFE tap coefficients, the array-based method described in [21] is used. An example for a six-tap FFE is given in Equation (2). Here, $a_{-2} \dots a_3$ denote the pre-, main- and post-cursors of the pulse response. The solution of the equation yields the tap coefficients $c_{-2} \dots c_3$ (with c_0 being the main tap filter coefficient).

$$\begin{bmatrix} a_0 & a_{-1} & a_{-2} & 0 & 0 & 0 \\ a_1 & a_0 & a_{-1} & a_{-2} & 0 & 0 \\ a_2 & a_1 & a_0 & a_{-1} & a_{-2} & 0 \\ a_3 & a_2 & a_1 & a_0 & a_{-1} & a_{-2} \\ 0 & a_3 & a_2 & a_1 & a_0 & a_{-1} \\ 0 & 0 & a_3 & a_2 & a_1 & a_0 \end{bmatrix} \cdot \begin{bmatrix} c_{-2} \\ c_{-1} \\ c_0 \\ c_1 \\ c_2 \\ c_3 \end{bmatrix} = \begin{bmatrix} 0 \\ 0 \\ 1 \\ 0 \\ 0 \\ 0 \end{bmatrix} \quad (2)$$

For the proposed digitally tunable FFEs a training sequence, shown in Figure 8a, is proposed. It contains all 12 possible pulse responses. The aforementioned matrix method can then be used to calculate coefficients for every response. Since the VCSEL is not linear, this method does not yield perfect results for the first iteration. To obtain more accurate results, the waveform was repetitively measured and the resulting coefficients were added to the previous ones until sufficient correlation was obtained. Figure 8b shows the 12 pulse responses overlaid after the coefficient training. Pre-, main- and post-cursors are marked by red circles and show excellent overlapping with the DC-levels.

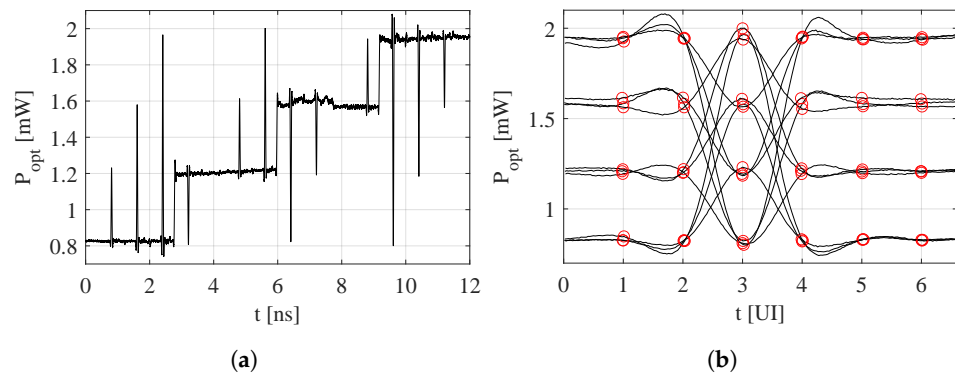


Figure 8. (a) Adaptive FFE training sequence, (b) overlaid pulse responses for all 12 combinations after training.

For the FFE using 4 sets of coefficients, the three responses for every level were normalized, and an average was formed, which then was used as a coefficient set.

5. Measurement Setup

A transmission experiment was performed to showcase the effectiveness of the adaptive FFEs. In this work 850 nm–940 nm oxide–confined GaAs VCSELs with an anti-waveguiding AlAs–rich core with apertures ranging from 3 μm to 7 μm [2] are used. This type of VCSEL enables highest reported bandwidths and thus enables very high data transmission under direct modulation. Figure 9 depicts the experimental measurement setup [22]. A 22 GHz bandwidth VCSEL wire-bonded to an RF connector and coupled into a lensed MMF fiber was used. It was connected to a Bias-T. The Bias-T combines an AC path, which is connected to an Arbitrary Waveform Generator (AWG) and a DC path, which is fed by a current source driving a bias current of 5 mA. The AWG is used to create a 2¹⁴ long, 800 mV_{pp} Pseudo-Random Binary Sequence (PRBS) which is pre-emphasized with a UI-spaced linear or adaptive FFEs with six Transmitter (TX) taps (two pre, one main, three post). The number of taps was chosen based on the length of the relaxation oscillations and the trade-off between better equalization (high amount of taps) and low computation complexity (low amount of taps). Since the filter effectively dampens the relaxation oscillations, increasing the amount of taps only gives diminishing returns after a certain number. The integrated 32 GHz receiver of the sampling oscilloscope is used to receive the optical signal of the VCSEL. For transmission experiments, OM-5 fiber was connected in-line. Synchronization of the system is attained by generating a clock signal with the second channel of the AWG, driving the phase reference module and trigger input of the sampling oscilloscope.

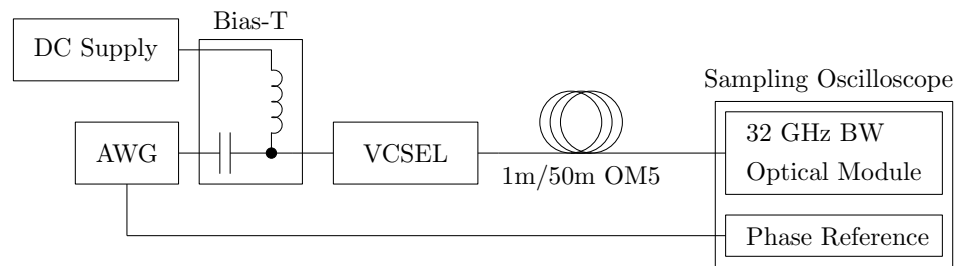


Figure 9. Experimental measurement setup.

BER performance was evaluated by exporting the Probability Density Function (PDF) eye diagram from the jitter and noise analysis software of the oscilloscope. Vertical bathtubs were calculated with the common method for Additive White Gaussian Noise (AWGN) channels of fitting normal distributions to the four PAM-4 levels and adding Q-functions [23]. The bathtub curves for every one of the three eyes were then combined into one vertical bathtub curve. This method of calculating BER is undertaken because commercially available stand-alone linear receivers have limited bandwidth and are difficult to de-embed, thus limiting the performance in combination with a bit-error tester.

6. Measurement Results and Discussion

In this section, the measurement results are shown and discussed. Figure 10 shows the resulting eye diagram for different forms of pre-emphasis.

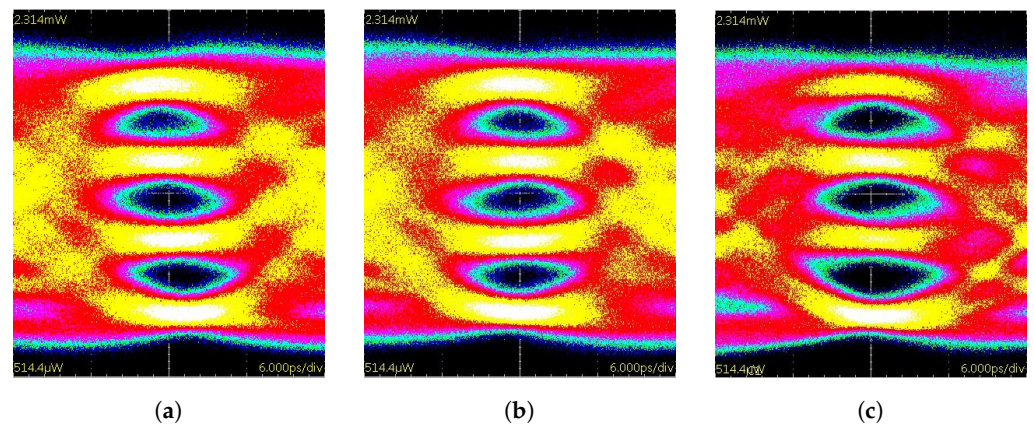


Figure 10. 80 Gbit/s eye diagrams using different pre-emphasis: 6 TX taps of, (a) linear FFE, (b) adaptive FFE with four sets of coefficients and (c) adaptive FFE with 12 sets of coefficients.

In Figure 10a, a linear FFE was used. Figure 10b,c illustrate the results for the proposed digitally tuned non-linear FFE with a set of 4 as well as 12 coefficients. All measurements were performed at a baud rate of 40 Gbaud. The average measured optical power was 1.4 mW for all three experiments. The adaptive structures are able to correct any skewing of the eyes. This was achieved by compensating the asymmetric rise-and-fall times through data-dependent pre-emphasis. To understand this effect, one can think of the VCSEL as an RC low-pass filter with a changing time constant. When a step function is applied, increasing the time constant of the filter can be counteracted by increasing the amplitude of the step, resulting in the same slew rate at the output. Although both adaptive structures are able to correct skewing, only the 12 sets of coefficient filter significantly increases the eye openings and achieves BER reduction. The BER reduces by a factor of 15, as shown in Table 2. When using four additional taps of Receiver (RX) equalization (added in the oscilloscope software), the effectiveness of the adaptive filter grows even bigger: The 12 coefficient filter achieves an over 30-fold decrease in BER in respect to the linear variant. Comparing the vertical bathtubs in Figure 11a–c, it is obvious that the skewing is mainly limiting the eye performance of the linear filter because the BER is dominated by the top

and bottom eye. Choosing a sub-par sampling point or large values of jitter would even amplify this effect since moving the sampling point to the right, the top eye’s BER would significantly increase, moving it to the left, the bottom eye would act accordingly. The four-coefficient filter (Figure 11b) is mostly limited by mid-and bottom eye performance. This could simply be due to the fact that the slicing time where optimum BER performance is reached is a little off center, or that the topmost eye is most open. Interestingly, the Ratio of Level Mismatch (RLM) performance shown in Table 2, varies a lot between the filters, even though DC levels were identical for all transmission experiments. The vertical bathtub using the 12 coefficient adaptive FFE shown in Figure 11c, shows that all three eyes share roughly the same BER at the optimal sampling point, making it less susceptible to jitter.

Table 2. Bit-Error Rates and RLM for different equalization settings at 40 Gbaud.

	TX EQ	no RX eq	4 Tap RX
BER	6Tap with 1 Coeff.	$9.9 \cdot 10^{-8}$	$8.1 \cdot 10^{-8}$
	6Tap with 4 Coeff.	$6.9 \cdot 10^{-8}$	$3.7 \cdot 10^{-8}$
	6Tap with 12 Coeff.	$6.7 \cdot 10^{-9}$	$2.6 \cdot 10^{-9}$
RLM	6Tap with 1 Coeff.	96.1%	95.9%
	6Tap with 4 Coeff.	93.7%	93.6%
	6Tap with 12 Coeff.	97.7%	98.1%

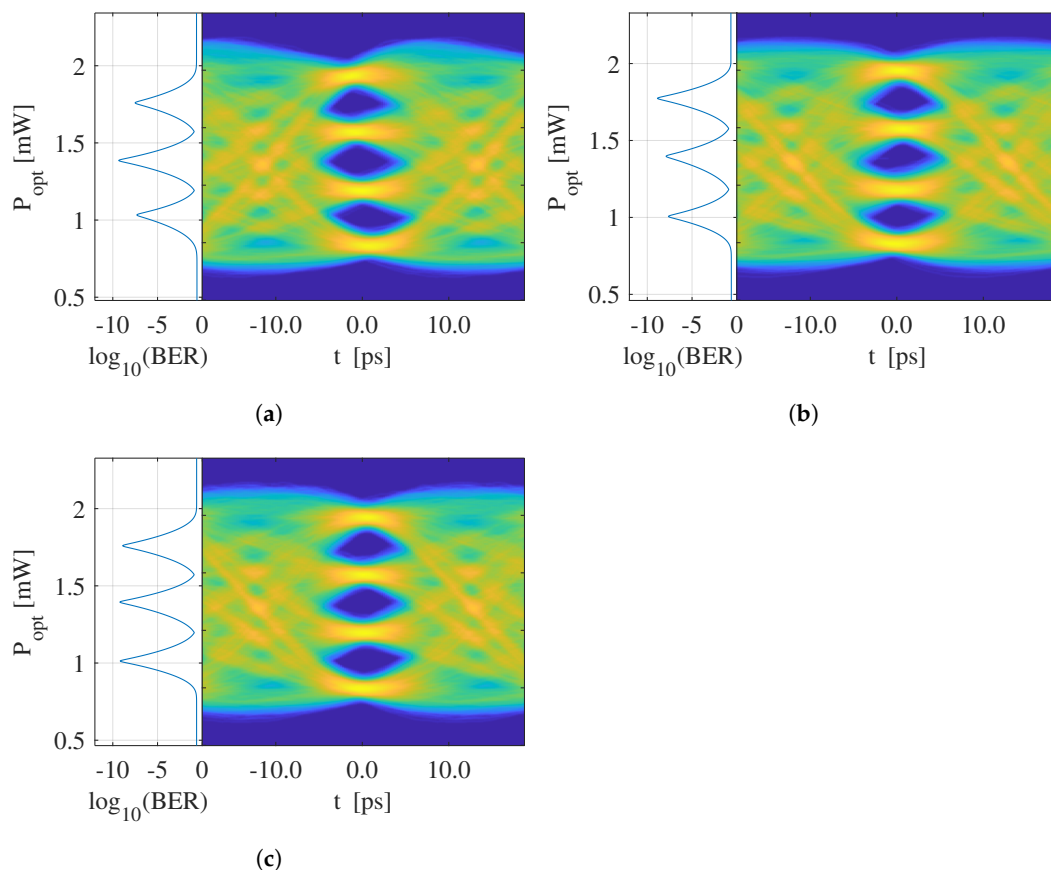


Figure 11. 80 Gbit/s eye diagrams with additional four taps linear FFE in the receiver using six TX taps of (a) linear FFE, (b) adaptive FFE with four sets of coefficients and (c) adaptive FFE with 12 sets of coefficients.

Since the adaptive FFE with 12 sets of coefficients proved to be most effective, it was also tested at a baud rate of 56 Gbaud. The measurement setup was changed by replacing the packaged and bonded VCSEL with a chip exhibiting a higher bandwidth of 28 GHz.

The optical device was mounted on a chuck, probed via a GS-probe and coupled into a fiber pigtail. Overall, the physical measurement setup was identical as in [24]. A total of seven taps were used in the transmit adaptive FFE and the VCSEL was biased with a bias current of 4.5 mA.

Figure 12a shows the output eye using the 12 coefficient adaptive FFE in the TX. It has an average optical output power of 1.8 mW. As before, the filter is again able to re-synchronize the eyes and remove skewing. When using 5 additional taps of linear equalization in the receiver (Figure 12b), the BER can be improved from $2.5 \cdot 10^{-6}$ to $1.5 \cdot 10^{-7}$. The transmission was also tested using 50 m of OM5 fiber, simulating the use in server-rack environment. Figure 12c reveals that the BER does not drop significantly for fiber lengths up to 50 m when using receiver equalization. In comparison to SOTA NRZ VCSEL drivers [6], a significant increase in data rate by a factor of $\approx 1.6x$ is achieved. Although the BER is quite a bit higher than 10^{-12} , it is still below the Forward Error Correction (FEC) threshold of $2.3 \cdot 10^{-5}$ for 3% overhead [25]. Incorporating the FEC overhead, an increase in data rate by a factor of $\approx 1.5x$ is reached.

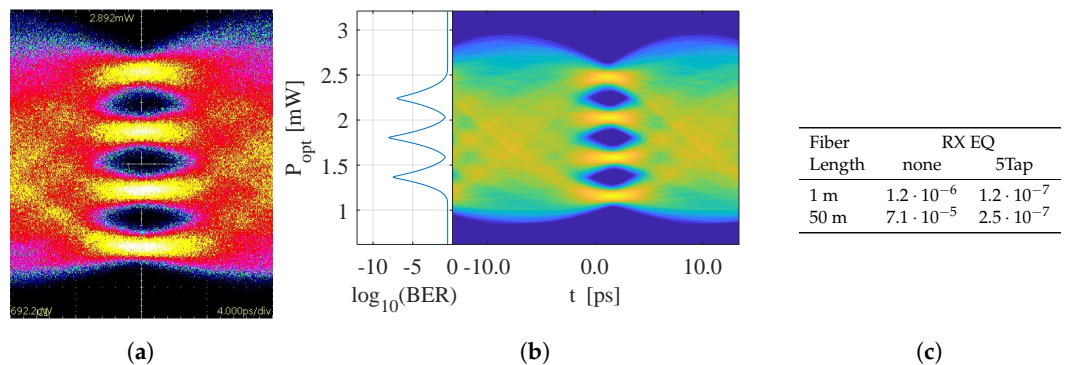


Figure 12. 112 Gbit/s eye diagrams using (a) no RX EQ and (b) 5 RX taps, (c) BER using different lengths of fiber.

7. Conclusions

This work demonstrated why VCSEL-based transmitter systems were not able to capitalize higher-order PAM modulation formats to advance the link data rate towards 100 Gbit/s with BER of better than 10^{-5} . The paper first explained the non-linear and biasing-dependent VCSEL behavior to prove why SOTA VCSEL transmitters including linear equalization were not able to reach these data rate targets. Consequently, a digitally enhanced non-linear transmit equalizer was proposed to overcome voltage-dependent relaxation frequency shifts as well as data-dependent VCSEL bandwidth variations. The proposed digital non-linear equalizer was compared with a standard linear FFE structure using PAM-4 transmission experiments of 100 Gbit/s and beyond. The proposed non-linear equalizer revealed a BER reduction of more than 30-fold compared to a linear FFE at a data rate of 80 Gbit/s. Using the proposed adaptive FFE with seven taps and additional five taps of RX equalization, data throughput of up to 112 Gbit/s was successfully demonstrated at a BER of approximately 10^{-7} . The suggested novel equalization scheme is fully implemented in the digital domain within integrated transmitter circuits taking advantage of energy-efficient lookup table realization with minor power and silicon area penalty.

Author Contributions: Conceptualization, U.H. and N.L.J.; methodology, P.K., H.O.; software, U.H. and P.K.; validation, U.H., N.L.J. and P.S.; formal analysis, F.G. and N.L.; investigation, U.H., N.L.J. and P.S.; resources, F.G. and N.L.; data curation, U.H. and N.L.J.; writing—original draft preparation, U.H.; writing—review and editing, N.L.J., H.O., P.K. and F.G.; supervision, F.G.; project administration, F.G.; funding acquisition, F.G. and N.L. All authors have read and agreed to the published version of the manuscript.

Funding: The authors would like to thank the Federal Ministry of Education and Research (BMBF) and the Fast Zwanzig20-Initiative for funding this work in the frame of the fast bits project —BMBF 03ZZ0525A. Some of the equipment used in this work was funded by the Deutsche Forschungsgemeinschaft (DFG, German Research Foundation)—INST 131/787-1 FUGG.

Institutional Review Board Statement: Not applicable.

Informed Consent Statement: Not applicable.

Data Availability Statement: Not applicable.

Conflicts of Interest: The authors declare no conflict of interest. The funders had no role in the design of the study; in the collection, analyses, or interpretation of data; in the writing of the manuscript; or in the decision to publish the results.

Abbreviations

The following abbreviations are used in this manuscript:

AC	Alternating Current
AWG	Arbitrary Waveform Generator
AWGN	Additive White Gaussian Noise
BER	Bit-Error Rate
CML	Current-Mode Logic
DAC	Digital-to-Analog Converter
DC	Direct Current
EML	Electro-Absorption Modulated Laser
FEC	Forward Error Correction
FFE	Feed-Forward Equalizer
FIR	Finite Impulse Response
ISI	Inter Symbol Interference
IoT	Internet-of-Things
LUT	Lookup Table
MMF	Multi-Mode Fiber
MZM	Mach-Zehnder-Modulator
NRZ	Non-Return to Zero
PAM	Pulse Amplitude Modulation
PDF	Probability Density Function
PRBS	Pseudo-Random Binary Sequence
RLM	Ratio of Level Mismatch
RX	Receiver
SOTA	State-of-the-Art
TX	Transmitter
UI	Unit Interval
VCSEL	Vertical-Cavity Surface-Emitting Laser

References

1. Cisco. *White Paper: VNI Complete Forecast Highlights 2022*; Technical Report; Cisco: San Jose, CA, USA, 2019.
2. Ledentsov, N.N.; Shchukin, V.A.; Kalosha, V.P.; Ledentsov, N.N.; Kropp, J.R.; Agustin, M.; Chorchos, Ł.; Stepniak, G.; Turkiewicz, J.P.; Shi, J.W. Anti-waveguiding vertical-cavity surface-emitting laser at 850 nm: From concept to advances in high-speed data transmission. *Opt. Express* **2018**, *26*, 445–453. [\[CrossRef\]](#)
3. Ledentsov, N.; Chorchos, Ł.; Agustin, M.; Ledentsov, N.N.; Turkiewicz, J.P. 850 nm single-mode VCSEL for error-free 60 Gbit/s OOK operation and transmission through 800 m of multi-mode fiber. In Proceedings of the Optical Fiber Communication Conference Postdeadline Papers 2019, San Diego, CA, USA, 3–7 March 2019; p. Th4B.6. [\[CrossRef\]](#)
4. Tian, S.C.; Mansoor, A.; Lindner, J.; Larisch, G.; Bimberg, D. High-power, single-mode, multi-aperture VCSELs for long-reach optical interconnects. In Proceedings of the 2021 Asia Communications and Photonics Conference (ACP), Shanghai, China, 24–27 October 2021; pp. 1–3.
5. Mansoor, A.; Tian, S.C.; Lindner, J.; Larisch, G.; Bimberg, D. Multi-aperture VCSELs: High power, low resistance, single mode. In Proceedings of the 2021 27th International Semiconductor Laser Conference (ISLC), Potsdam, Germany, 10–14 October 2021; pp. 1–2. [\[CrossRef\]](#)

6. Kuchta, D.M.; Rylyakov, A.V.; Doany, F.E.; Schow, C.L.; Proesel, J.E.; Baks, C.W.; Westbergh, P.; Gustavsson, J.S.; Larsson, A. A 71-Gb/s NRZ Modulated 850-nm VCSEL-Based Optical Link. *IEEE Photonics Technol. Lett.* **2015**, *27*, 577–580. [[CrossRef](#)]
7. Chorchos, L.; Ledentsov, N.; Kropp, J.R.; Shchukin, V.A.; Kalosha, V.P.; Lewandowski, A.; Turkiewicz, J.P.; Ledentsov, N.N. Energy Efficient 850 nm VCSEL Based Optical Transmitter and Receiver Link Capable of 80 Gbit/s NRZ Multi-Mode Fiber Data Transmission. *J. Light. Technol.* **2020**, *38*, 1747–1752. [[CrossRef](#)]
8. *IEEE Std. 802.3bs-2017*; IEEE Standard for Ethernet Amendment: Media Access Control Parameters for 800 Gb/s and Physical Layers and Management Parameters for 400 Gb/s and 800 Gb/s Operation. IEEE: New York, NY, USA, 2022.
9. Broadcom. *Broadcom's 100 Gbps VCSEL and 200 Gbps EML Enable Next-Generation 1.6 Tbps Pluggable Optics*; Broadcom: San Jose, CA, USA, 2022.
10. Hwang, J.; Choi, H.S.; Do, H.; Jeong, G.S.; Koh, D.; Park, K.; Kim, S.; Jeong, D.K. A 64 Gb/s 2.29 pJ/b PAM-4 VCSEL Transmitter with 3-Tap Asymmetric FFE in 65 nm CMOS. In Proceedings of the 2019 Symposium on VLSI Circuits, Kyoto, Japan, 9–14 June 2019; pp. C268–C269. [[CrossRef](#)]
11. Soenen, W.; Vaernewyck, R.; Yin, X.; Spiga, S.; Amann, M.C.; Steenberge, G.V.; Mentovich, E.; Bakopoulos, P.; Bauwelinck, J. 56 Gb/s PAM-4 Driver IC for Long-Wavelength VCSEL Transmitters. In Proceedings of the ECOC 2016—42nd European Conference on Optical Communication, Dusseldorf, Germany, 18–22 September 2016; pp. 1–3.
12. Chen, J.; He, Z.S.; Lengyel, T.; Szczerba, K.; Westbergh, P.; Gustavsson, J.S.; Zirath, H.; Larsson, A. An Energy Efficient 56 Gbps PAM-4 VCSEL Transmitter Enabled by a 100 Gbps Driver in 0.25 m InP DHBT Technology. *J. Light. Technol.* **2016**, *34*, 4954–4964. [[CrossRef](#)]
13. Belfiore, G.; Khafaji, M.; Henker, R.; Ellinger, F. A compact electro-optical VCSEL model for high-speed IC design. In Proceedings of the 2016 12th Conference on Ph.D. Research in Microelectronics and Electronics (PRIME), Lisbon, Portugal, 27–30 June 2016; pp. 1–4. [[CrossRef](#)]
14. Bjerkan, L.; Royset, A.; Hafskjaer, L.; Myhre, D. Measurement of laser parameters for simulation of high-speed fiberoptic systems. *J. Light. Technol.* **1996**, *14*, 839–850. [[CrossRef](#)]
15. Gao, Y.; Cartledge, J.C.; Yam, S.S.H.; Rezania, A.; Matsui, Y. 112 Gb/s PAM-4 Using a Directly Modulated Laser with Linear Pre-Compensation and Nonlinear Post-Compensation. In Proceedings of the ECOC 2016—42nd European Conference on Optical Communication, Dusseldorf, Germany, 18–22 September 2016; pp. 1–3.
16. Huang, W.J.; Chang, W.F.; Wei, C.C.; Liu, J.J.; Chen, Y.C.; Chi, K.L.; Wang, C.L.; Shi, J.W.; Chen, J. 93 ℓ_1 -Regularization for 112-Gbps PAM-4 850-nm VCSEL Optical Interconnect. In Proceedings of the 2018 Optical Fiber Communications Conference and Exposition (OFC), San Diego, CA, USA, 11–15 March 2018; pp. 1–3.
17. Belfiore, G.; Szilagyi, L.; Henker, R.; Ellinger, F. 25 Gbit/s adaptive 3-tap FFE VCSEL driver in 28-nm CMOS for data center communications. In Proceedings of the 2017 19th International Conference on Transparent Optical Networks (ICTON), Girona, Spain, 2–6 July 2017; pp. 1–4. [[CrossRef](#)]
18. Belfiore, G.; Khafaji, M.; Henker, R.; Ellinger, F. A 50 Gb/s 190 mW Asymmetric 3-Tap FFE VCSEL Driver. *IEEE J. Solid-State Circuits* **2017**, *52*, 2422–2429. [[CrossRef](#)]
19. Raj, M.; Monge, M.; Emami, A. A Modelling and Nonlinear Equalization Technique for a 20 Gb/s 0.77 pJ/b VCSEL Transmitter in 32 nm SOI CMOS. *IEEE J. Solid-State Circuits* **2016**, *51*, 1734–1743. [[CrossRef](#)]
20. Hecht, U.; Ledentsov, N.; Scholz, P.; Agustin, M.; Schulz, P.; Ledentsov, N.N.; Gerfers, F. Non-Linear PAM-4 VCSEL Equalization and 22 nm SOI CMOS DAC for 112 Gbit/s Data Transmission. In Proceedings of the 2019 12th German Microwave Conference (GeMiC), Stuttgart, Germany, 25–27 March 2019; pp. 115–118. [[CrossRef](#)]
21. Lee, S.M.; Sim, J.Y.; Park, H.J. An analytic decision method for the feed-forward equalizer tap-coefficients at transmitter. In Proceedings of the 2009 International SoC Design Conference (ISOC), Busan, South Korea, 22–24 November 2009; pp. 400–403. [[CrossRef](#)]
22. Hecht, U.; Ledentsov, N.; Chorchos, L.; Kurth, P.; Ledentsov, N.N.; Gerfers, F. Up to 30-Fold BER Improvement using a Data-Dependent FFE Switching Technique for 112 Gbit/s PAM-4 VCSEL Based Links. In Proceedings of the 2020 Optical Fiber Communications Conference and Exhibition (OFC), San Francisco, CA, USA, 8–12 March 2020; pp. 1–3.
23. Proakis. *Digital Communications 5th Edition*; McGraw Hill: New York, NY, USA, 2007; pp. 160–190.
24. Hecht, U.; Ledentsov, N.; Chorchos, L.; Scholz, P.; Schulz, P.; Turkiewicz, J.P.; Ledentsov, N.N.; Gerfers, F. 120 Gbit/s multi-mode fiber transmission realized with feed forward equalization using 28 GHz 850 nm VCSELs. In Proceedings of the 45th European Conference on Optical Communication (ECOC 2019), Dublin, Ireland, 22–26 September 2019; pp. 1–4. [[CrossRef](#)]
25. Sakib, M.N.; Liboiron-Ladouceur, O. A Study of Error Correction Codes for PAM Signals in Data Center Applications. *IEEE Photonics Technol. Lett.* **2013**, *25*, 2274–2277. [[CrossRef](#)]

Disclaimer/Publisher's Note: The statements, opinions and data contained in all publications are solely those of the individual author(s) and contributor(s) and not of MDPI and/or the editor(s). MDPI and/or the editor(s) disclaim responsibility for any injury to people or property resulting from any ideas, methods, instructions or products referred to in the content.